Materials & Design 267 (2026) 116375

Contents lists available at ScienceDirect

Materials & Design

journal homepage: www.elsevier.com/locate/matdes

Grain boundary hardening vs softening in nanocrystalline CuZn30

Oliver Leon Petry [a,*], Enrico Bruder [a], Marcel Sos [a], Julian Mathias [a], Yuting Dai [b,c], Matthias Schwotzer [c], Christian Kübel [b,c,d], Karsten Durst [a]

[a] Physical Metallurgy, Department of Materials and Earth Sciences Technical University of Darmstadt, Darmstadt, Peter-Grünberg-Straße 2, 64287 Darmstadt, Germany
[b] In-situ Electron Microscopy, Department of Materials and Earth Sciences, Technical University of Darmstadt, Peter-Grünberg-Straße 2, 64287 Darmstadt, Germany
[c] Institute of Nanotechnology, Karlsruhe Institute of Technology, Hermann-von-Helmholtz-Platz 1, 76344 Eggenstein-Leopoldshafen, Germany
[d] Karlsruhe Nano Micro Facility (KNMFi), Karlsruhe Institute of Technology, Hermann-von-Helmholtz-Platz 1, 76344 Eggenstein-Leopoldshafen, Germany

ARTICLE INFO

Keywords:
Ultrafine-grained
Nanocrystalline, strain rate jump
Brass
High pressure torsion
Thermomechanical

ABSTRACT

Nanocrystalline (NC) and ultrafine-grained (UFG) materials are known for increased mechanical strength compared to their coarse grained (CG) counterparts. However, at elevated temperatures softening as well as enhanced strain rate sensitivity can be observed in NC and UFG materials. In this study the different effects of temperature, strain rate and strain on the microstructure and mechanical strength of NC and CG CuZn30 are investigated. High pressure torsion (HPT) is used to produce bulk samples of nanocrystalline CuZn30. Tensile, compression and nanoindentation tests are employed to investigate the mechanical properties at temperatures up to 300 °C. This study shows the strengthening effect of GBs at RT and the softening effect at elevated temperatures. It is shown that the microstructure is thermomechanically stable at temperatures up to 150 °C and that the softening at these temperatures is fully reversible. At higher temperatures, a transient regime can be observed where the NC material softens further, but deformation driven grain growth leads to coarsening. The Coble creep, Blum-Zeng and Figueiredo-Langdon models are compared to experimental data for the strain rate sensitivity exponent m. The best agreement was found for the Figueiredo-Langdon model, which fits well for the stable temperature regime from RT up to 200 °C.

1. Introduction

In recent years the interest in nanocrystalline (NC) and ultrafine-grained (UFG) metals and alloys has increased because of their unique properties. The increased volume fraction of grain boundaries (GBs) in these materials strongly influences functional and structural properties such as electrical conductivity, wear resistance, and mechanical strength. [1–5] Severe plastic deformation (SPD) processes like equal channel angular pressing (ECAP) or high pressure torsion (HPT) can be used to produce dense bulk samples of ultrafine grained (UFG) or even nanocrystalline (NC) microstructures in metals and alloys [6,7]. During SPD a material dependent saturation grain size is reached. In single phase alloys, the saturation grain size shows a strong dependence on the solid solution hardening (SSH) contribution, with higher SSH leading to smaller grain sizes [6,8–10]. According to the Hall-Patch relation such fine structured alloys show very high strength while still maintaining good compressive ductility. However, it is known that at elevated temperatures UFG and NC materials can show lower strength than their coarse-grained (CG) counterparts, displaying a change from GB hardening towards GB softening or breakdown of the Hall-Petch effect [11,12]. Furthermore, an increased strain rate sensitivity (SRS) can be observed in fine grained materials, showing lower strength at lower strain rates. This increase in SRS is even more pronounced at elevated temperatures. [11,12].

In contrast the CG microstructure shows no temperature or strain rate sensitivity but displays work hardening, which results in the formation of subgrains composed of low angle grain boundaries (LAGBs). However, the microstructure that is formed after SPD is mostly composed of high angle grain boundaries (HAGBs) [13]. The difference between the NC material and a deformed CG material is therefore not only in the volume fraction of the GBs (which can be estimated at 1–2 % for a grain size of 100 nm, assuming a GB thickness of 1 nm [13–15]) but also in the character of the GBs.

There are several models which try to explain the breakdown of the Hall-Petch effect for very small grain sizes, based on dislocation mechanisms, grain boundary-shearing mechanisms, diffusion mechanisms, or

* Corresponding author at: Physical Metallurgy, TU Darmstadt, Peter-Grünberg-Straße 2, 64287 Darmstadt, Germany.
E-mail address: oliver.petry@tu-darmstadt.de (O.L. Petry).

https://doi.org/10.1016/j.matdes.2026.116375
Received 12 December 2025; Received in revised form 16 May 2026; Accepted 8 June 2026
Available online 9 June 2026

two-phase models [16]. At elevated temperatures the Hall-Petch breakdown can be described best by a diffusion-based model, assuming a temperature sensitive mechanism becoming the dominant deformation mechanism[17]. Different models can be discriminated on the basis of temperature, grain size and strain rate dependence. The Blum-Zeng model and Coble creep are two extreme cases for the stress to grain size relation, with d^3 (coble creep) and $d^{-1/2}$ (Blum-Zeng model). Coble creep in a process that describes self-diffusion along the GB making it most relevant for small grain sizes. The Blum-Zeng model describes the strengthening of the material by the rate at which dislocations are stored at high angle grain boundaries (HAGB). In CG materials the mean free path of dislocations depends on the subgrain size w_{CG} [18] but in a fine grained material with $d \leq w_{CG}$ dislocations are stored at GBs and not in the grain interior [19,20]. The softening at elevated temperatures is the result of enhanced recovery of dislocations at HAGBs due to fast climb rates of edge dislocations at GBs [19,20].

The model described as grain-boundary sliding model by Figueiredo and Langdon [21–23] assumes a steady state between dislocation recovery and generation. Like the Coble creep the relation between grain size and stress is d^3. The model simulates dislocation glide along GBs and the formation of dislocation pile ups at triple junctions. After sufficient stress build up dislocations advance through the opposing grain on a different slip system until they reach a GB. At the GB dislocations climb until they are absorbed into the GB. This model is valid under the assumption that there are no subgrain boundaries and the dislocations can glide through the grain, which is true for a NC microstructure.

The Coble creep and Blum-Zeng model assume different strain rate sensitivities, $m = 1$ for the Coble creep and $m = 1/8$ for the Blum-Zeng model [24]. The Figueiredo-Langdon model assumes a strain rate sensitivity exponent of $m = 0.5$ for low stresses, but this value decreases for high stresses. Therefore, testing at different strain rates e.g. strain rate jump (SRJ) experiments may be suitable to discriminate between underlying deformation mechanisms in the models. While the Figueiredo-Langdon model introduces a temperature-dependent SRS, there are also limitations.

The Figuero-Langdon model considers the sum of a GB-sliding component, which only incorporates grain size effects and a threshold stress component which is a simple estimation of other strengthening mechanisms (representing the flow stress of a single crystal). [25]The estimation of the threshold stress in this model is very limited, which is why the models are only used and discussed for the strain rate sensitivity, where the threshold stress is assumed constant. [26].

The goal of this study is to investigate GB hardening vs. softening in NC CuZn30 at elevated temperatures and compare the results with CG counterpart. There are multiple studies on the temperature dependent deformation behavior in UFG and NC Cu, Al, and Ni. [11,12,27] However, in these studies the microstructure stability is not guaranteed at elevated temperatures. CuZn30 is a well-known alloy and the addition of Zn increases the thermal stability of the microstructure, allowing mechanical testing at elevated temperatures, while as a single-phase material there are no additional effects from secondary phases. The HPT process ensures high density bulk samples, avoiding any influence of porosity. For the mechanical characterization, uniaxial tensile and compression tests as well as high temperature scanning indentation (HTSI) are used at temperatures up to 300 °C. The results contribute towards a generalized concept describing the mechanical properties of NC materials. The challenge when investigating NC materials is their metastable character. Especially at elevated temperatures recovery and recrystallization processes will influence mechanical measurements. Furthermore, the addition of stress and strain during mechanical testing can assist grain growth, leading to enhanced grain growth and grain growth at lower temperatures [28–30].

2. Experimental

Disk shaped CuZn30 (Table 9 1) samples were deformed up to saturation employing a HPT machine by Walter Klement GmbH. The samples had an initial height of $h_1 = 2mm$ and $h_2 = 4.5mm$ both types of samples had a diameter of 20 mm. During the HPT process a force of 1450 kN was applied, corresponding to a pressure of 4.6 GPa. The torsional deformation was applied with a speed of $v = 1rpm$ using 25 rotations for samples with a height of $h_2 = 4.5mm$ and 12 rotations for samples with a height of $h_1 = 2mm$, achieving a van Mieses strain of 58 000 %. During the HPT processing, the upper anvil is cooled with water, keeping the temperature close to RT. After the HPT processing the thinner samples had a height of $h_{HPT1} = 1.3mm$ while the thicker had a height of $h_{HPT2} = 3.3mm$.

For the assessment of the thermal stability a NC CuZn30 disk was cut into multiple pieces, ensuring the same initial conditions. The sample pieces then received an isochronal heat treatment at different temperatures (T = RT, 100 °C, 150 °C, 200 °C, 250 °C, 300 °C, 400 °C, 600 °C) for one hour. SEM-BSE images were taken perpendicular to the rotation axis of the HPT, at a radius of 5 mm. The grain size was determined using the line interception method. By analyzing the grain growth after annealing, the activation energy Q can be calculated using:

$$ln\left(\frac{d^n - d_0^n}{t}\right) \propto \left(-\frac{Q}{R}\right) \bullet \frac{1}{T} \tag{1}$$

With D being the grain size, D_0 the initial grain size, n the grain growth exponent, R the gas constant, T the temperature and t the time.

Compression samples were cut out of cylinders lying next to the HPT-disk center (Fig. 9 1). Tensile samples were cut from HPT samples after grinding to a thickness of 1 mm. Out of each disk-shaped sample two tensile samples were cut avoiding the center (Fig. 9 2) which does not reach saturation grain size during HPT. The gauge length was determined using a confocal laser-microscope and measured at 6 mm while the width was 1.5 mm. Before testing the edges were rounded using SiC 500 grinding paper.

Macroscopic compression and tensile tests are performed using an Instron Universal Testing System 5967 with a 30 kN load cell and an environmental chamber for tests at elevated temperatures. For the comparison of thermomechanical and thermal influence on the mechanical properties and microstructure a reference sample is placed inside the climate chamber during the whole testing procedure, experiencing the same temperature history as the mechanically tested sample. The strain rate sensitivity exponent m is determined from strain rate jump experiments using the following equation:

$$m_{a\to b} = \frac{ln(\sigma_{mean,a}) - \ln(\sigma_{mean,b})}{ln(\dot{\varepsilon}_a) - \ln(\dot{\varepsilon}_b)} \tag{2}$$

Nanoindentation experiments were conducted using a G200 nanoindentation system by Keysight equipped with a diamond Berkovich tip (Synton-MDP). A depth dependent hardness is recorded using a continuous stiffness method (CSM) based on a method by Oliver and Pharr [31]. This method uses a constant indentation strain rate, while for the evaluation of the strain rate sensitivity an indentation SRJ test according to Maier et al. [32] was employed. The indentation rate was changed after every 500 nm displacement into the surface. As in the macroscopic compression tests where a change in strain rate leads to a change in yield strength, there is a change in hardness when changing the indentation rate. The strain rate sensitivity exponent can then be calculated [32] using the following expression:

$$m_{nanoindentaion} = \frac{(\delta \ln H)}{(\delta \ln \dot{\varepsilon}_{indentation})} \tag{3}$$

To account for pile-up formation, the hardness is calculated based on Sneddon's equation [31] (Eq.4). Sneddon's hardness is calculated from the harmonic contact stiffness S:

$$S = \frac{2\beta}{\sqrt{\pi}} \bullet E_R \bullet \sqrt{A_c} \tag{4}$$

where E_R is the reduced modulus, A_c is the contact area, and β is a constant, which depends on the geometry of the indenter [31,33]. For the indenter used in this work $\beta = 1$. Employing Eq.4 to calculate the contact area gives the corrected hardness based on the contact stiffness:

$$H = \frac{P}{A_c} = \frac{4 \bullet \beta^2}{\pi} \bullet \frac{E_R^2}{S^2} \tag{5}$$

where P is the applied load.

High temperature scanning indentation experiments were performed from RT-200 °C to compare SRS values from different methods. For these measurements a KLA HT1K nanoindenter was employed [34]. The indenter system is mounted inside a TESCAN VEGA3 SEM and testing was carried out under vacuum (10^{-4} Pa). The HTSI tests were performed during thermal ramping (heating & holding) following the procedure described by Tiphene et al. in [35] and Sos et al. in [36].

For the evaluation of the microstructure, BSE-SEM images are used and the line interception method. Additionally, automated crystal orientation mapping (ACOM) is used. For ACOM, CuZn30 samples were cut to 80 nm thickness using a FEI Strata 400S focused ion beam/scanning electron microscope (FIB/SEM) system, with the lamella positioned parallel to the plane view of the disk. Precession electron diffraction (PED) experiments for ACOM were performed with the NanoMegas ASTAR system, using a precession angle of 0.6°. For that, the microscope was operated in micro-probe STEM mode with a convergence angle 0.5 mrad and a camera length of 245 mm to acquire the diffraction patterns. This setup results in a nominal beam diameter of about 1.5 nm. The maps were acquired with 5 nm step size.

3. Results

3.1. Microstructure stability

The BSE-SEM and ACOM images taken for each sample are displayed in Fig. 3 1. The microstructure after HPT is compared to that of annealed samples and samples that have experienced mechanical deformation at elevated temperatures.

The microstructure of the reference state right after HPT shows an average grain size of 105 nm (line interception method) with a standard deviation of about 31 nm. The saturation grain size corresponds to the material specific saturation grain size of $CuZn_{30}$ that is found after HPT processing [13,37]. Annealing at 100 °C has no observable influence on the microstructure (Fig. 3 1b). ACOM shows that after HPT the fraction of HAGBs is more than 75 %, which does not change during annealing at temperatures up to 200 °C (Table 3 1).

After annealing at 300 °C the microstructure shows significant coarsening and parallel GBs can be observed (formation of annealing twins) [38,39]. This is confirmed by ACOM: The amount of HAGBs increases to 97 % and the number of twin boundaries increases to 45 % at 300 °C. While ACOM measurements result in larger grain sizes due to the different calculation method, the stability of the microstructure up to 200 °C is confirmed. Annealing at higher temperatures leads to accelerated grain growth, with an increase by one magnitude after annealing at 300 °C and another magnitude after annealing at 600 °C. Fig. 3 2 shows the hardness and grain size as a function of the annealing temperature after one hour.

Initially an increase in hardness can be observed from 2.49 GPa to 2.64 GPa after annealing at 100 °C and to 2.66 GPa after annealing at 200 °C. This increase in hardness after annealing at low temperatures is known as hardening via annealing and is attributed to a reduced number of mobile dislocations [40,41]. Annealing at 300 °C leads to a significant

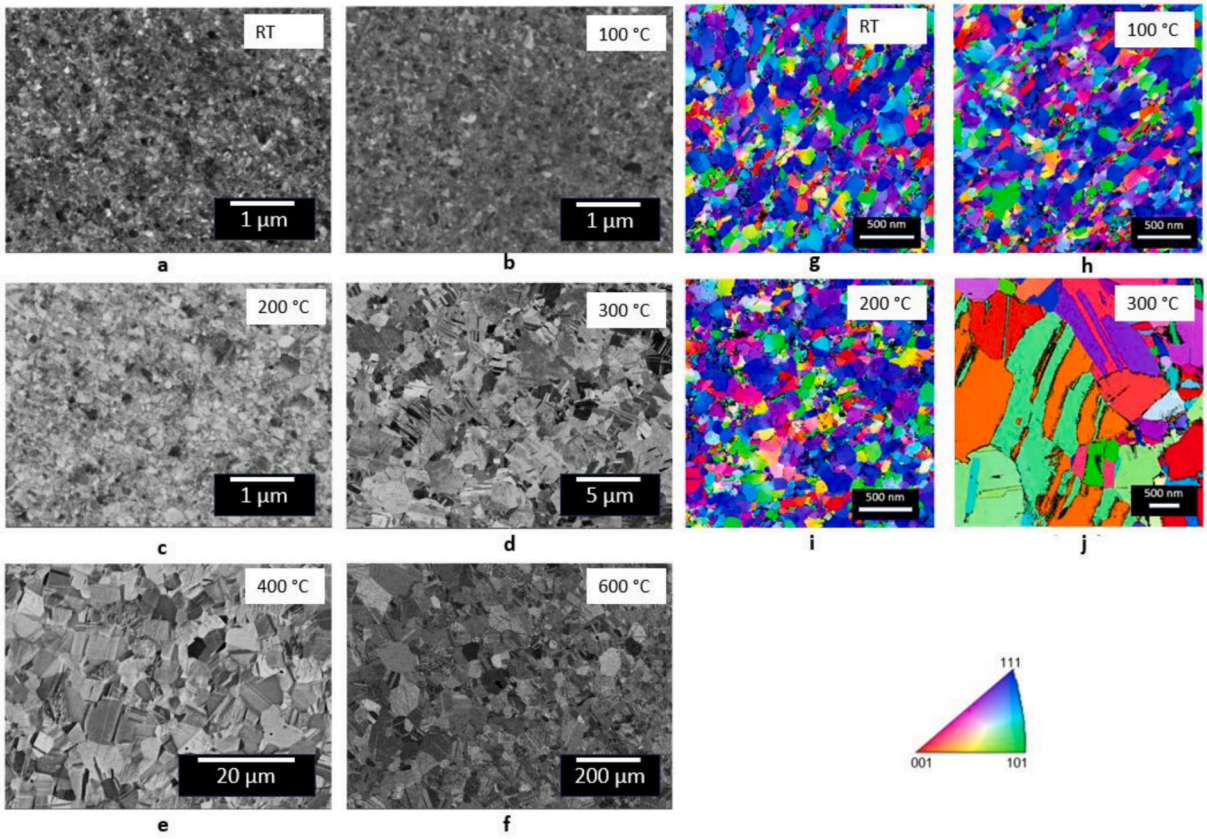

Fig. 3 1. SEM-BSE (left) and ACOM (right) images of samples after isochronal annealing for 1 h at indicated temperature.

Table 3 1
Fraction of lagb, hagb and twins as well as area weighted grain size for different annealing temperatures, taken from acom measurements and grain size from bse images using the line interception method.

	LAGB (%)	HAGB (%)	TWIN (%)	Area weighted grain size (μm)	Line interception method grain size (μm)
HPT reference	23 ± 2	77 ± 2	19 ± 1	0.168 ± 0.097	0.105 ± 0.031
100 °C, 1 h	27 ± 1	73 ± 1	17 ± 2	0.155 ± 0.090	0.110 ± 0.031
200 °C, 1 h	27 ± 1	73 ± 1	17 ± 2	0.163 ± 0.089	0.111 ± 0.030
250 °C, 1 h	27	73	19	0.226 ± 0.194	0.371 ± 0.060
300 °C, 1 h	3	97	45	1.050 ± 0.680	1.325 ± 0.279

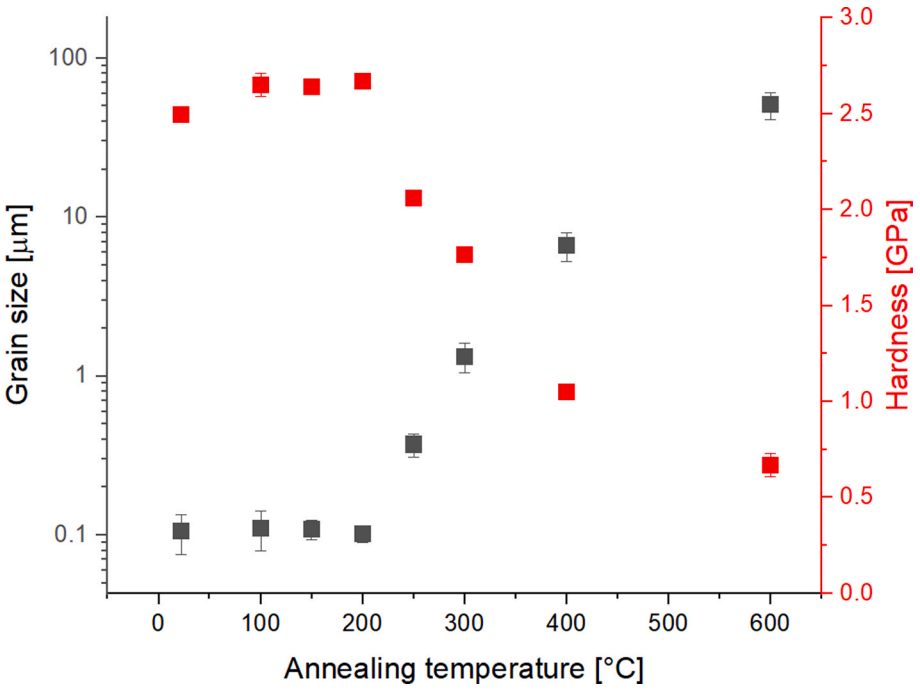

Fig. 3 2. Hardness after isochronal annealing (red) and grain size using the line interception method (black) of CuZn30 vs. isochronal annealing temperature. (For interpretation of the references to colour in this figure legend, the reader is referred to the web version of this article.)

drop in hardness to 1.71 GPa. After annealing at 600 °C for one hour the grain size increased by two orders magnitudes and the hardness drops to 0.66 GPa, which corresponds to about 27 % of the initial state.

Differential scanning calorimetry (DSC) (Fig. 3 3) shows a first exothermic peak around 200 °C (0.35 T/T_m). However, there is no significant change in grain size observable after annealing at 200 °C. The exothermic peak, which is observed in the DSC measurement can most likely be attributed to GB relaxation processes and the annealing of vacancies and dislocations, which has no effect on the grain size. This phenomenon is also observed in other FCC NC copper alloys [42,43]. The DSC measurement after annealing at 200 °C shows a shift towards higher temperatures, while the first exothermic peak becomes narrower. The relaxation processes below 200 °C are mostly finished which means there are no further transitions at those temperatures.

Between 250 °C and 300 °C there is a tenfold increase in grain size observable, reaching an average grain size of 1 ± 0.18 μm. These observations indicate recrystallization processes that start somewhere between 200 and 300 °C. After annealing at 300 °C there is no longer a visible peak, indicating complete recrystallization. Annealing at 400 °C shows that the grain size increases further, which is an indicator for ongoing grain growth.

Fig. 3 4 shows the microstructure of NC CuZn30 samples after strain rate jump tests at 150 °C and 200 °C, in comparison with a reference sample. At 150 °C there is no visible difference in the microstructure between just the thermal treatment and the added compressive strain. However, at 200 °C an increase in grain size can be observed.

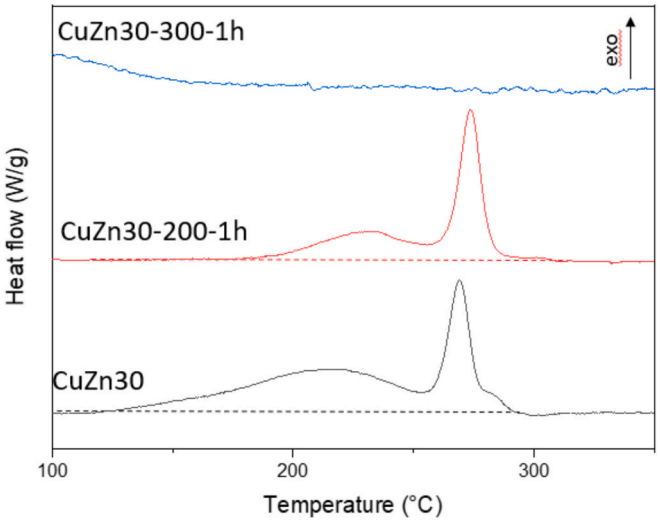

Fig. 3 3. . Differential scanning Calorimetry on CuZn30 after HPT (black), after annealing at 200 °C (red), and after annealing at 300 °C (blue) for one hour. (For interpretation of the references to colour in this figure legend, the reader is referred to the web version of this article.)

EBSD measurements of a CG CuZn30 compression sample after 20 %

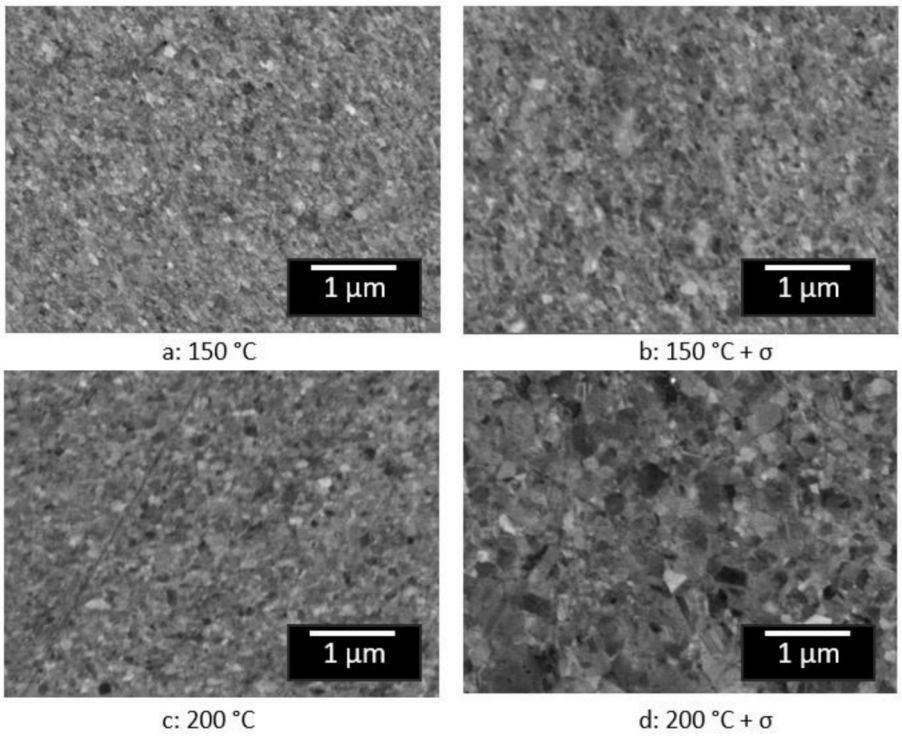

Fig. 3 4. BSE images after annealing at indicated temperature (a + c) and compression tests at indicated temperature (b + d).

strain show a grain size of about 100 µm. Furthermore, subgrain boundaries are visible as well as twin boundaries. These structures become clearer in the Kernel average misorientation (KAM) map. Fig. 3 5 reveals that some grains accommodate large amounts of deformation in the form of twinboundaries, while accommodate for less deformation. It seems like grains closer to the 001 orientation accommodate more stress, but a higher sample size is necessary for a reliable result. The average subgrain size lies at about 40 µm, but varies between 50 µm and 20 µm, depending on the grains that are observed.

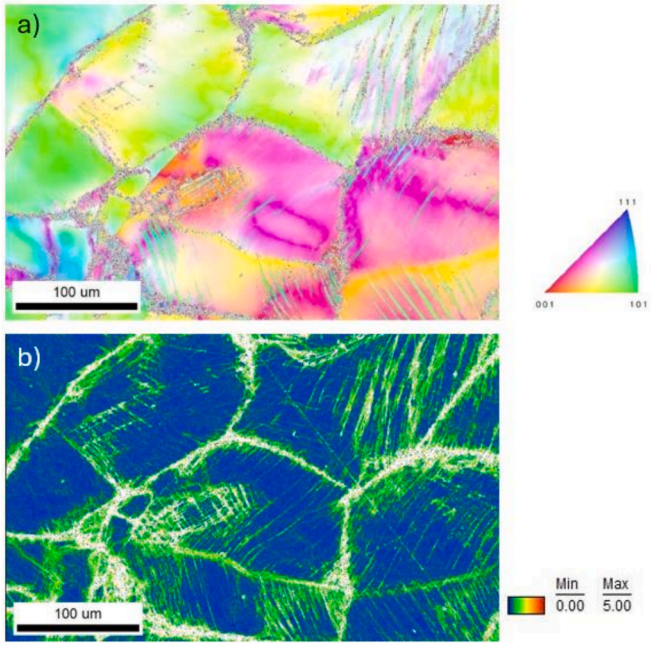

Fig. 3 5. EBSD measurements of CG CuZn30 after 20 % compressive deformation. a) crystal orientation, b) average misorientation.The measurement was taken in the middle of the sample orthogonal to direction of stress.

3.2. *Mechanical testing*

Uniaxial compression tests at elevated temperatures show the hardening and softening effect an increased number of GBs has in NC materials compared to their CG counterparts. Furthermore, strain rate jump tests can be used to calculate the strain rate sensitivity.

3.2.1. *Uniaxial compression tests*

Fig. 3 6 shows the stress–strain compression curves at a constant strain rate ($10^{-3}\,s^{-1}$) of nanocrystalline and CG $CuZn_{30}$ at RT and elevated temperatures (100, 200 and 300 °C). The 0.2 % yield strength is

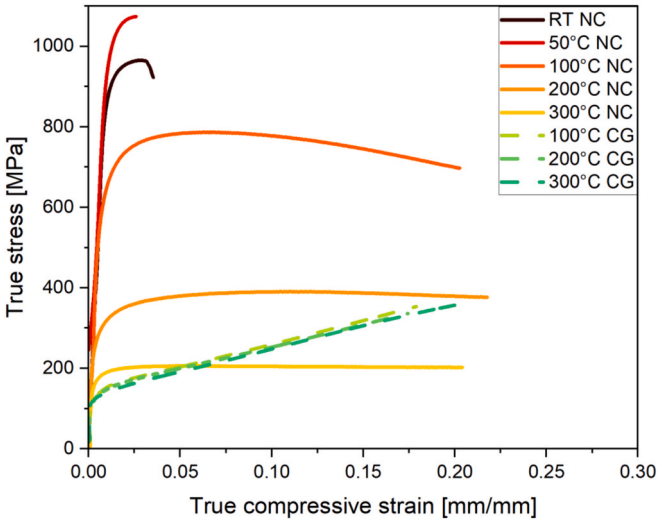

Fig. 3 6. True compressive stress–strain curves of nanocrystalline (nc) and coarse-grained (CG) samples at RT- 300 °C with a constant strain rate of $10^{-3}\,s^{-1}$.

used as a measure for comparisons between the NC material and the coarse-grained material. At RT the yield strength of CG CuZn30 is measured as 120 MPa and shows no significant change at elevated temperatures. In comparison, the yield strength of the NC sample increases approximately sevenfold with 860 MPa at RT. However, the yield strength of the NC material shows a strong temperature dependence. The yield strength drops to 600 MPa at 100 °C and to 280 MPa at 200 °C.

The stress–strain curves of all NC samples show an inflection (a region with low or no work hardening) resulting in a plateau. The CG samples show an almost linear increase of strength in the plastic regime due to work hardening, increasing from about 100 MPa to almost 360 MPa at 20 % strain. Using the Taylor equation, it is possible to estimate the dislocation density.

$$\sigma = M\alpha Gb\sqrt{\rho} \tag{6}$$

With the critical shear stress τ, a geometric constant α, the burgers vector b and the shear modulus G. Assuming a shear modulus of G = 40 GPa, a burgers vector of b = 2.55 Å, a Mecking Kocks constant $\alpha = 0.3$ [44], and a Taylor factor M = 3.06 for FCC polycrystals, the dislocation density at 20 % strain is estimated as $\rho \approx 1.5 \bullet 10^{15} m^{-2}$.

The strength and work hardening effects do not change significantly at elevated temperatures. In contrast the NC samples show a plateau that is reached after small compressive strains of about 2.5 %. At 300 °C the strength of NC samples drops below that of CG samples, as can be seen in Fig. 3 6, which can be interpreted as a breakdown of the Hall-Petch-Effect.

The strain rate sensitivity exponent m is determined using equation (2). The mean value for the stress is determined in the range of $[\varepsilon_{end} - \Delta, \varepsilon_{end}]$, where Δ is adjusted depending on the shape of the curve. For an approximately horizontal curve$\Delta = 0.01$ is used, in any other case$\Delta = 0.005$.

SRJ tests reveal a high strain rate sensitivity in the NC alloys. For higher strain rates an increased strength can be observed, while a decrease in strain rate leads to a decrease in strength. This behavior is even more pronounced at elevated temperatures. At 200 °C the strength varies by 100 MPa as the strain rate is changed by one order of magnitude. Furthermore, the strength does not change instantaneously as does the strain rate, but instead shows a transient range [11,32]. The transient region also increases slightly with increasing temperature. SRJ test on CG samples (Fig. 3 7) show no significant influence of temperature or strain rate on the mechanical behavior of the material. Only some discontinuities when changing the strain rate can be observed. At RT the NC CuZn30 show shearing failure for strain rates of 10^{-3}, which makes a reliable evaluation of SRJ compression tests difficult.

The average strain rate sensitivity exponents from HTSI measurements, SRJ compression and nanoindentation tests are displayed in Fig. 3 8. Additionally, the stress exponent n = 1/m is plotted on a secondary y-axis. The results for Nanoindentation at RT are in good agreement with literature where the same method was used [13,37]. HTSI measurements show the same values at RT and slightly lower values for m at elevated temperatures, compared to compression tests. Both methods show an increase of m by an order of magnitude from RT to 200 °C. HTSI data stops at 200 °C, since at higher temperatures Zn will start to evaporate at the surface under vacuum. For comparison the results with the models in literature, the SRS exponents are included, with m = 1 for Coble creep and m = 0.25 for the Blum-Zeng model. The strain rate sensitivity according to the Figueiredo-Langdon model can be calculated using the following equations [26]:

$$m = \frac{\alpha\beta\dot{\varepsilon}}{2(\beta\dot{\varepsilon}+1)\sqrt{\alpha \ln(\beta\dot{\varepsilon}+1)}\left(\sqrt{\alpha \ln(\beta\dot{\varepsilon}+1)} + \sigma_0\right)} \tag{7}$$

Where α describes the GB sliding:

$$\alpha = \frac{\sqrt{3}GkT}{2db^2} \tag{8}$$

And

$$\beta = \frac{d^3}{2\delta D_{gb}} \tag{9}$$

Where G = shear modulus, k = Boltzmann constant, T = absolute temperature, d = grain size, b = Burgers vector (b = 0.256 nm), δ= GB width ($5.12 \bullet 10^{-10}$), D_{gb} = GB diffusion coefficient ($D_0 = 5 \bullet 10^{-15} m^3/s$, $and Q_{gb} = 104 kJ/mol$), and σ_0 is a threshold stress assumed to be constant (10 MPa). [26] α describes the GB sliding contribution and β dictates whether superplasticity or Hall-Petch behavior may be expected. For large GB diffusion and small grainsizes β becomes very small and GB sliding dominates. [25]

Compression strain rate jump tests for all included temperatures are displayed in Fig. 9 4. Tensile test results are shown in Fig. 9 3.

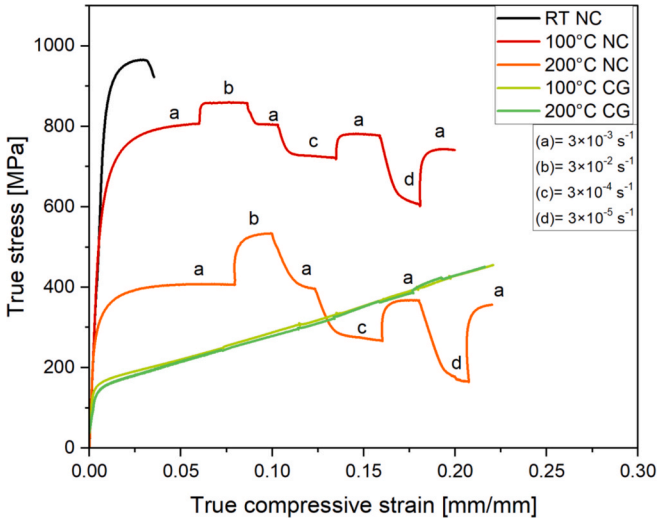

Fig. 3 7. Stress–strain curves with SRJs at 100 °C and 200 °C of NC and CG samples.

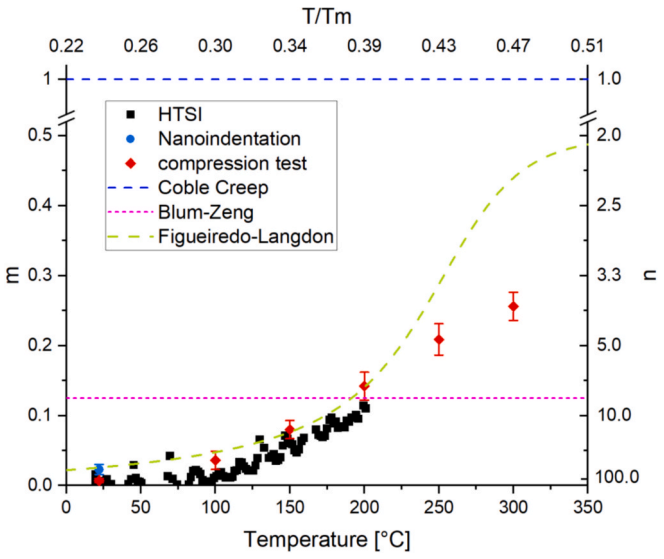

Fig. 3 8. SRS exponent m and stress exponent n over temperature (homologous temperature T/T_m) from HTSI measurement as well as compression and nanoindentation SRJ experiments in comparison with Coble creep, Blum-Zeng and Figueiredo-Langdon models.

4. Discussion

Experiments have shown that the hardening effect of GBs changes towards a softening at elevated temperatures, eventually reaching a condition where the NC material becomes softer than the CG material at high temperatures and low strain rates. In the following these observations are discussed regarding the stability of the microstructure and the expectations from models like the Blum-Zeng model.

4.1. Thermal and thermomechanical stability

By analyzing the grain growth after annealing, the activation energy Q can be calculated using equation (1). The theoretical value for the grain growth exponent n is approximately 2 for pure metals at temperatures close to the melting point [39]. However, this assumes an ideal single-phase material. Any deviations from the ideal material can have strong influences on grain growth since the driving force for grain growth is very small. Some of those deviations can be changes in grain size distribution, the presence of texture or small amounts of second phase or other pinning defects. In literature the grain growth exponent for α-brass is given as 3.7 [45], which is the value used for the calculation in this case.

As can be seen in Fig. 4 1 the Arrhenius plot shows two different regions with different activation energies. The first region at low temperatures shows a low activation energy which could be attributed to GB relaxation processes without significant grain growth. This is also in agreement with the DSC measurement (Fig. 3 3). After SPD a fraction of the GBs is in a so-called deformation affected state. These GBs are characterized by higher diffusivities along the GB and pronounced strain fields compared to random high angle grain boundaries (HAGBs) in a relaxed state [41,46–48]. In the higher temperature regime, the activation energy is close to the activation energy of bulk diffusion in α-brass [49–51]. This would indicate diffusion processes to be the mechanism behind grain growth.

When investigating the softening at elevated temperatures it is necessary to differentiate between the influence of temperature and mechanical stress on the microstructure. For testing temperatures of up to 150 °C no significant change in microstructure between the mechanically tested samples and the reference sample could be observed (Fig. 4 2). Therefore, it can be assumed that the microstructure is not

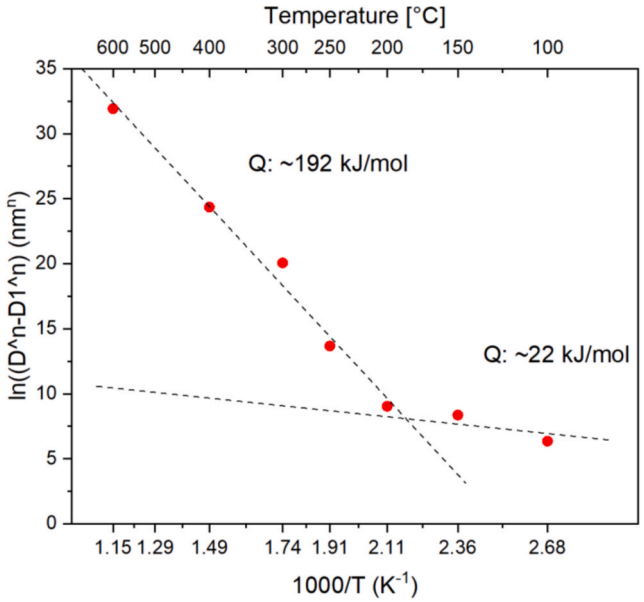

Fig. 4 1. Arrhenius plot of ln(D^n −D$_1$^n) vs. 1000/T to estimate the activation energy for grain growth Q of the CuZn30 samples.

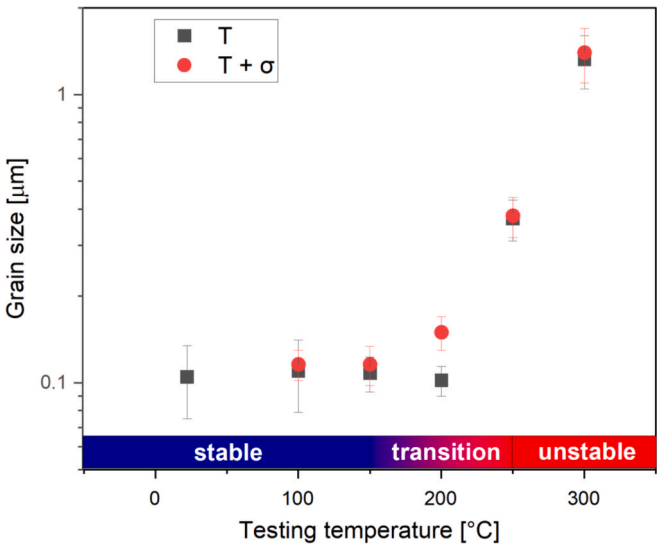

Fig. 4 2. Grain size after SRJ tests at different temperatures (red) compared to reference samples subject to the same thermal conditions (grey). Scale at the bottom shows stable temperature regime, transition (thermally but not thermomechanically stable) and unstable regime. (For interpretation of the references to colour in this figure legend, the reader is referred to the web version of this article.)

only thermally but also thermomechanically stable.

At 200 °C, the sample with additional mechanical treatment shows an increase in grain size compared to the reference sample. Although, the microstructure is thermally stable after annealing at 200 °C, the grains size increases to 150 nm after conducting a SRJ test at the same temperature, indicating a transition between the stable and unstable temperature regime where the microstructure is thermally but not thermomechanically stable. This observation could be attributed to stress assisted grain growth or deformation enhanced grain growth. Stress assisted grain growth has been observed in UFG copper, where it could even be observed at cryogenic temperatures [29]. The grain growth was found to be higher at cryogenic temperatures, where the applied stress was higher, leading to the conclusion that it is a stress-driven mechanism. However, in this case, coarsening increased at elevated temperatures, where lower stresses were applied. Deformation enhanced grain growth of UFG microstructures in aluminum could be observed by Mey et al. after compression tests at elevated temperatures, similar to the conditions in this experiment [12]. It was suggested that the grain growth results from mobile subgrain boundaries, that migrate and dissolve while high-angle GBs stay unchanged. Another approach was taken by Valiev et al., who could observe grain growth in UFG copper after deformation during compression tests. It is suggested that during deformation the activation energy for grain growth is lowered [28]. A reduced activation energy fits well with the observation that the relative difference in grain size between thermally and thermomechanically treated samples becomes negligible at higher temperatures. However, further studies are necessary to evaluate the relevant mechanisms.

4.2. Grain boundary hardening vs. Softening

At RT the increase in yield strength from 120 MPa in the CG material to 860 MPa in the NC material can be calculated with the Hal-Petch relation given in equation (10).[52]

$$\sigma_0 = \sigma_i + K_H d^{-1/2} \tag{10}$$

Whereσ_0 = the yield stress, σ_i = friction stress, K_H is the Hall-Petch constant which measures the relative hardening contribution of the

GBs and d = grain diameter. Assuming σ_i lies between 50–80 MPa and $K_H = 220 - 250 MPa\mu m^{-1/2}$ for brass [53], the yield stress should be 80–120 MPa for the CG material and 750–870 MPa for the NC material, which fits with the measurement results.

It has been shown that the strength and hardness of NC CuZn30 decrease significantly at elevated temperatures, while the strain rate sensitivity increases. Furthermore, this behavior is not a result of a changing microstructure, which is stable for temperatures up to 200 °C and up to 150 °C under deformation. The influence of the increase in grain size from 105 nm to 150 nm during deformation at 200 °C (Fig. 4 2) can be calculated using the Hall-Petch relation (equation (10). This would account for a yield strength reduction of 140 MPa. However, the total strength reduction is approximately 580 MPa.

Plotting the strength of NC and CG CuZn30 after 20 % plastic deformation for different strain rates and temperatures (Fig. 4 3), reveals the change towards a diffusion-controlled deformation mechanism at elevated temperatures.

The CG material is largely unaffected by the strain rate and only shows a slight drop in strength with temperature. The NC material initially shows an increase in strength at 50 °C, which might be a result of hardening via annealing, which leads to an increase in strength before the deformation mechanism changes leading to the softening at higher temperatures. However, to fully understand this phenomenon requires further investigation beyond the scope of this work. Between 50–100 °C the deformation mechanism changes, which can be considered a breakdown of the Hall-Petch effect. As already established in the introduction, due to the small average distance between GBs in NC materials, the rate limiting processes that determine the macroscopic deformation mechanism, take place around the GBs. This aligns with simulations that predict a low dislocation density in the grain interior for small grain sizes. [19,54].

In Fig. 4 3 for each different strain rate a crossing point of similar strength between NC material and CG counterpart can be identified. This could be an indicator for similar dislocation structures (grain size vs. subgrain size) in NC and CG materials. EBSD measurements indicate an average subgrain size of about 40 µm in the CG material with 20 % strain. However, the subgrain size varies strongly between different grains. Some grains show large amounts of deformation with twin GBs and subgrain sizes of about 20 µm. Considering a larger area of influence from a subgrain boundary of several Burgers vectors (compared to the thickness of HAGBs in the NC microstructure), the influenced volume would be smaller by several orders of magnitude.

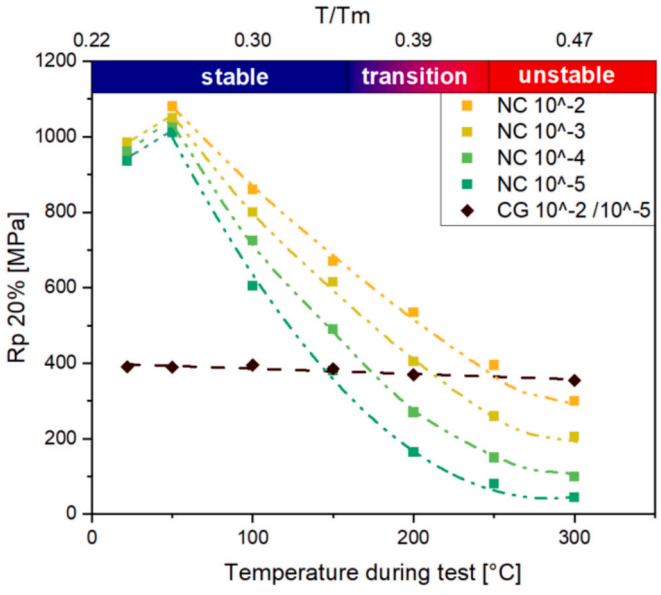

Fig. 4 3. Strength at 20 % plastic strain of NC and CG CuZn30 vs. testing temperature for different strain rates, taken from uniaxial compression tests.

The small grain size in the NC material leads to pile ups of dislocations at the GBs, which enhances dislocation annihilation due to smaller distances between annihilation partners. [19,55] At low homologous temperatures the result is an increase in strength according to the Hall-Petch relation, with GBs acting as barriers for dislocation movement, resulting in GB hardening. At high homologous temperatures the strength drops, because the deformation is now controlled by the thermally driven annihilation and recovery rate of dislocations, resulting in GB softening. [19,32,56,57] A strong temperature dependence of strength and strain rate sensitivity has already been demonstrated in fcc metals, specifically for pure copper and pure aluminum [11,12]. However, the microstructure showed coarsening during the measurements. Using Zn and Sn as alloying materials to stabilize NC Cu-X alloys, Sos et al. [36] observed softening in UFG CuZn5 and NC CuSn5 using HTSI. Similar to the experiments with CuZn30 the softening effect was completely reversible at temperatures up to 200 °C.

In comparison to pure Cu, CuZn30 does not only have the additional SSH contribution and consequently smaller saturation grain size, but the addition of 30 wt% Zn lowers the SFE from ~45 mJ/m^2 to ~14 mJ/m^2 and the melting temperature to 1228 K. [58] A low SFE is associated with more stable dislocation structures, by suppressing cross-slip and dynamic recovery, which could influence dislocation-GB interaction. The NC alloys CuZn5 (T_m = 1338 K) and CuSn5 (T_m = 1333 K), investigated by Sos et al. [36] have SFE close to that of pure Cu with 43 mJ/m^2 and 40 mJ/m^2 respectively. CuSn5 is much more stable showing the Hall-Petch breakdown at a homologous temperature of 0.35 T/T_m, while the breakdown in CuZn30 is at 0.28 T/T_m and CuZn5 already shows the onset of the softening at RT (0.23 T/T_m). Since the SFE is higher in both CuSn5 and CuZn5, no conclusions regarding the influence of the SFE can be drawn from these results. However, the SSH contribution and saturation grain size seem to influence the thermomechanical stability of the alloys, with higher SSH (smaller saturation grain size) resulting in higher stability and a shift of the Hall-Petch breakdown towards higher homologous temperatures.

The SRJ experiments at these temperatures show that the transient range after a SRJ, until a stable state (stress in the case of the compression tests and hardness in the case of nanoindentation) is reached, broadens with increasing temperature. This behavior is well known in literature and is caused by the thermally activated time-dependent dislocation and GB migration. [56,59] Fig. 3 8 shows the increase of the SRS exponent m with increasing temperature.

From the SRJ data it is possible to directly calculate an apparent activation volume Ω for each temperature using equation (11) [27,60]:

$$\Omega = \sqrt{3} \bullet k_B T \bullet \frac{\partial \ln(\dot{\varepsilon})}{\partial \sigma} = \sqrt{3} \bullet k_B T \bullet \frac{m}{\sigma} \tag{11}$$

where Ω is the apparent activation volume, k_B the Boltzmann constant, T the temperature, $\dot{\varepsilon}$ the strain rate, m the strain rate sensitivity exponent and σ the stress. It should be noted that the apparent activation volume is different from the true activation volume, as it not only reflects the thermally activated event but also depends on the current stress level. Since the stress level decreases strongly with temperature, the apparent activation volume changes even if the underlying mechanism does not change. [27,59] Table 4 1 displays the values for the activation volume

Table 4 1
0.2 % proof stress, strain rate sensitivity exponent m, stress exponent n, activation volume and grain size d of NC CuZn30 at different temperatures.

Temperature [K]	$Rp_{0.2}$ (10^{-3} s^{-1}) [MPa]	m	n	Ω[b^3]	d [nm]
295	860	0.007 ± 0.003	143	20.86	105
373	600	0.036 ± 0.013	28	15.19	110
473	280	0.142 ± 0.02	7	9.15	111
573	160	0.26 ± 0.02	3.8	13.32	1325

at different temperatures ranging between 9–21 b^3, which is consistent with thermally activated dislocation GB interaction, as opposed to forest dislocation cutting (which would give$\Omega \sim 100$–$1000\ b^3$). [27,57] Asaro and Suresh [60] predict an activation volume of 3–10 b^3 for truly NC metals, increasing monotonically with grain size. This is consistent with our findings (9–21 b^3) for grain sizes at the upper end of the NC regime (100 nm).

At 300 °C the activation volume sees again an increase from 9 b^3 to 13 b^3. This behavior can be attributed to the onset of grain growth observed at this temperature (Table 4 1). Since the activation volume for GB-mediated dislocation interaction scales with grain size, the coarsening toward the UFG regime naturally raises Ω. However, the change in activation volume is small. At these temperatures multiple processes take place inside the grain and any interpretation should be taken with care.

At 200 °C the experimentally determined value for m is approximately 1/8, which is the value assumed in the Blum-Zeng model. However, the Blum-Zeng model assumes a fixed value for m, as does the coble creep model in which $m = 1$ for diffusional creep. [19,20,24] The Figueiredo-Langdon model fits well with experimental data up to temperatures of 200 °C. At higher temperatures thermally activated grain growth is expected, which not only changes the grain size but the introduction of subgrain boundaries (increased number of twins Table 3 1) invalidates the model.

With the constant strain rate data and the m values calculated from SRJ compression tests (Table 4 1), the apparent activation energy for the rate controlling deformation mechanism can be estimated using [27,60]:

$$Q_{app} = -\frac{k_B \bullet T^2}{m \bullet \sigma}\left(\frac{\partial \sigma}{\partial T}\right)_{\dot{\varepsilon}} \tag{12}$$

With the values for the 0.2 % proof stress at $\dot{\varepsilon} = 10^{-3}s^{-1}$ and m from Table 4 1 three intervals can be evaluated (Table 4 2) using mean values for T, m and σ. Just as for the apparent activation volume, since the flow stress level decreases with temperature, the apparent activation energy is expected to decrease even if the underlying deformation mechanism does not change. Therefore, the calculated values should be treated as representative activation energies to determine the dominant mechanism at each temperature interval, not as material constants. [27,59]

In the first regime (RT-100 °C) the activation energy is at 197 kJ/mol close to that of bulk diffusion for α-brass (~192 kJ/mol). [49,51] However, at these low temperatures the relative error of the strain rate sensitivity exponent is very high and the apparent activation energy is directly proportional to 1/m (equation (12). This small value for m also indicates a nearly athermal mechanism (m→0 or n ≈ 100 indicating athermal dislocation glide). In the second regime (100 °C-200 °C), where the microstructure is confirmed to be stable, the apparent activation energy lies between that of bulk diffusion and GB diffusion in α-brass (~80–90 kJ/mol). This fits with the idea of dislocation climb assisted by the enhanced diffusivities along non-equilibrium HAGB [41,46–48]. In the third regime (200 °C-300 °C) the apparent activation energy decreases to a level smaller than that of GB diffusion in Cu (62 kJ/mol). The activation energy for GB diffusion from literature is given for recrystallized microstructures with equilibrium GBs resulting in the higher value compared to the activation energy calculated here. Nonetheless these results point toward diffusion-controlled plasticity in agreement with n-values approaching n = 3–5, as discussed before. The progressive drop in activation energy with temperature is consistent with observations by Wang et al. [27]who reported this behavior for NC Ni (30 nm).

Further investigation into the dislocation structures and GB relaxation processes in the NC and CG material are necessary to develop a generalized concept that predicts the mechanical properties of nanostructured materials at RT and elevated temperatures, including influences of strain rate, grain size and chemical composition.

Table 4 2
Apparent activation energy for three intervals (RT-100 °C; 100 °C-200 °C; 200 °C-300 °C), including error calculation based on the standard deviation of m Table 4 1.

Temperature interval	T_{mean} [K]	T_{mean}/T_m	Q_{app} [kJ/mol]	Q_{app} [eV]
RT→100 °C	373	0.27	197 ± 82	2.04 ± 0.85
100 °C→200 °C	473	0.35	122 ± 19	1.26 ± 0.2
200 °C→300 °C	573	0.43	62 ± 6	0.65 ± 0.06

5. Conclusion

A brass alloy (CuZn30) was severely deformed by HPT until the saturation state was reached. The resulting nanocrystalline CuZn30 alloy has a saturation grain size of 105 nm and is thermally stable up to temperatures of 200 °C. ACOM measurements confirm a high fraction of HAGBs with more than 70 %. The properties of HAGBs are very temperature sensitive, leading to softening and increased strain rate sensitivity even at low homologous temperatures. This is reflected in the increased strain rate sensitivity exponent at elevated temperatures, increasing by an order of magnitude from RT (0.01) to 200 °C (0.12). At temperatures up to 150 °C the microstructure is completely stable and the softening fully reversible. At a temperature of 200 °C and a strain rate of $\dot{\varepsilon} = 10^{-3}$ the strength of the NC (105 nm) alloy drops below the value of the CG (40 μm) alloy at 20 % strain. It could be shown that the microstructure shows some deformation induced grain growth at 200 °C increasing to d = 150 nm. However, a Hall-Petch analysis showed that less than 25 % (140 MPa) of the observed softening (580 MPa) can be attributed to the coarsening of the microstructure. This suggests that the softening and increased strain rate sensitivity at elevated temperatures are primarily caused by the interactions between HAGBs and dislocations. Three models were compared with experimental data regarding the development of the SRS exponent with increasing temperature. The Figueiredo-Langdon model shows the best agreement including the temperature and strain rate dependence of the SRS exponent. However, further research into the kinetics of dislocation accommodation and stress relaxation processes at GBs is necessary to develop a complete model for the description of the mechanical properties of NC materials at elevated temperatures. Furthermore, the influence of the alloying components which influence saturation grain size and thermal stability should be investigated in further works towards a generalized model.

CRediT authorship contribution statement

Oliver Leon Petry: Writing – original draft, Investigation, Formal analysis. **Enrico Bruder:** Writing – review & editing, Supervision, Project administration. **Marcel Sos:** Writing – review & editing, Resources, Data curation. **Julian Mathias:** Investigation, Data curation. **Yuting Dai:** Investigation, Data curation. **Matthias Schwotzer:** Resources. **Christian Kübel:** Writing – review & editing, Validation. **Karsten Durst:** Writing – review & editing, Supervision, Project administration, Investigation, Funding acquisition, Conceptualization.

Declaration of competing interest

The authors declare that they have no known competing financial interests or personal relationships that could have appeared to influence the work reported in this paper.

Acknowledgements

This work was funded by the German Research Foundation (DFG) under grant number 497284200. The authors thank Dr. Achim Kuhn (Wieland-Werke AG, Germany) for providing the CuZn30 solid solution. Furthermore, the authors thank Matthias Schwotzer (Karlsruhe Institute

of Technology*)* for the contribution of DSC measurements.

Appendix

CuZn30 composition

.

Table 9 1
CuZn30 composition (Chemical analysis).

Element	Results [mas.-%]	Deviation U ± [mas.-%]
Zn	***29,6107***	0,204
Pb	***0,0058***	0,0008
Sn	***0,0019***	0,0023
P	***0,0048***	0,0002
Mn	***<0,001***	----
Fe	***<0,0015***	----
Ni	***0,0023***	0,0018
Si	***<0,002***	----
Mg	***<0,0005***	----
Cr	***<0,0005***	----
As	***0,0054***	0,0005
Sb	***0,0064***	0,0006
Cd	***0,0006***	0,0003
Bi	***<0,005***	----
Co	***0,0046***	0,0009
Al	***<0,0006***	----
S	***0,0010***	0,0006
Cu	***70,3***	0,21

6.1. Compression sample geometry

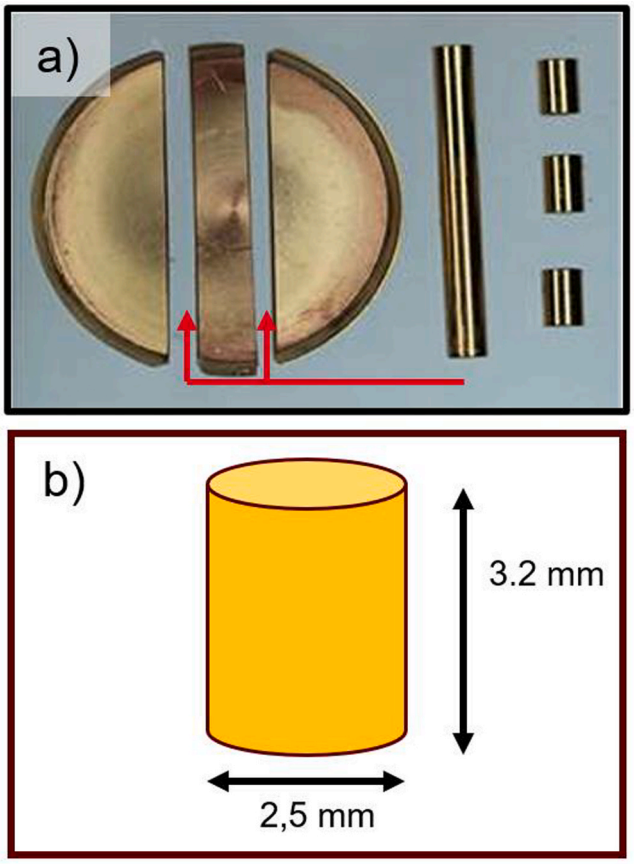

Fig. 9 1. a)HPT sample and compression sample cutout, b) compression sample geometry.

6.2. Tensile sample geometry

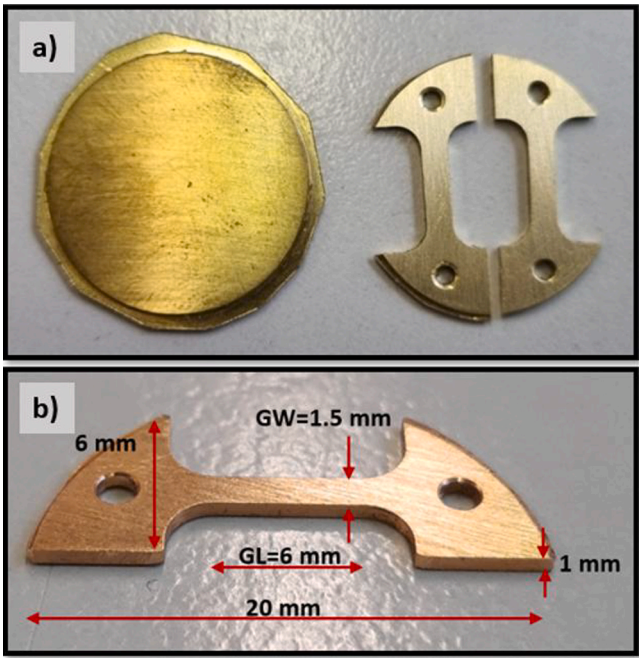

Fig. 9 2. a) HPT sample and Tensile sample cutout, b) Tensile sample geometry.

6.2.1. Tensile tests

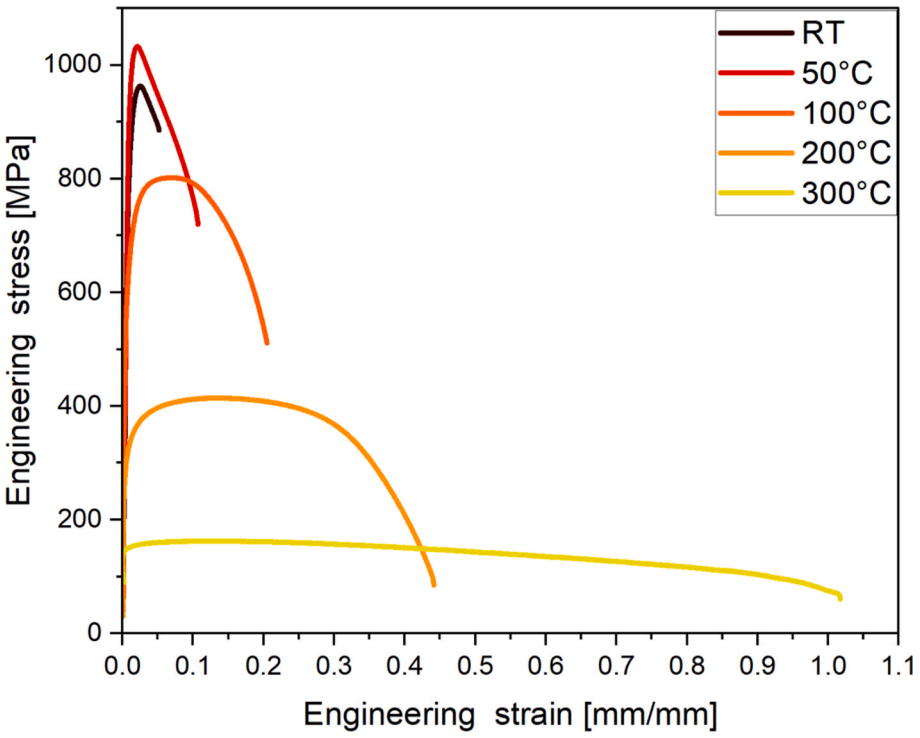

Fig. 9 3. Engineering stressstrain curve of NC CuZn30 at RT, 100°C and 200°C during tensile test.

At RT the Yield strength is at 800 MPa and the material shows a low ductility. At 100 °C the yield strength slightly drops to 600 MPa and at 200 °C it significantly drops to 290 MPa. Furthermore, the ductility increases significantly with rising temperature. At RT necking starts shortly after reaching yield strength. However, at 100 °C, an inflection can be observed, reaching a strain of about 0.07 before ultimate tensile stress (UTS) is reached. This behavior is even more pronounced at 200 °C where twice the strain is reached, before UTS is reached. At 300 °C the ductility increases significantly as can be seen from the sample images. However, it should be noted, that at this temperature the microstructure can no longer be considered uniform over the whole experiment, since the isothermal annealing has shown recrystallization starting around 250 °C.

6.3. Compression SRJ

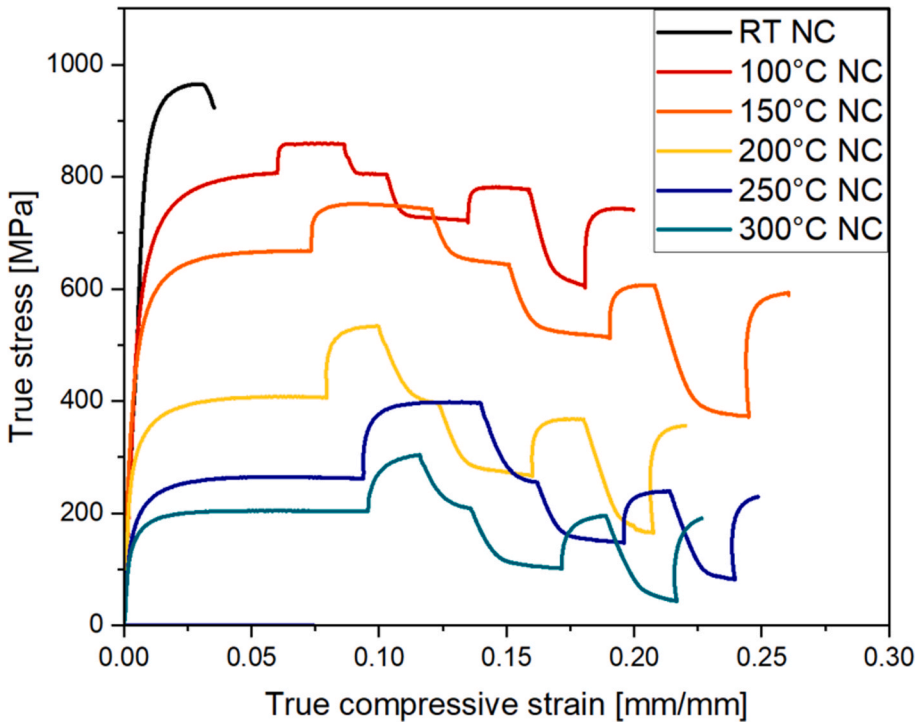

Fig. 9 4. Compression SRJ for NC CuZn30 (RT-300°C).

Data availability

Data will be made available on request.

References

[1] J.E. González-Hernández, J.M. Cubero-Sesin, Electrical conductivity of ultrafine-grained Cu and Al alloys: attaining the best compromise with mechanical properties, Mater. Trans. 64 (8) (2023) 1754–1768.

[2] H. Ha, S. Ko, B. Goh, S. Müller, R.-P. Baumann, M. Leem, S. Jo Yoo, J. Choi, B. Hwang, Influence of grain boundary density on the surface energy of nanocrystalline metal thin films, Appl. Surf. Sci. 604 (2022) 154463.

[3] M.Y. Murashkin, D.I. Sadykov, A.M. Mavlyutov, V.U. Kazykhanov, N.A. Enikeev, Effect of Mg content on mechanical properties and electrical conductivity of ultrafine-grained Al–Mg–Zr wires produced by ECAP-Conform and drawing, J. Mater. Sci. 59 (14) (2024) 5923–5943.

[4] A.K. Kushwaha, M. John, M. Misra, P.L. Menezes, Nanocrystalline materials: synthesis, characterization, properties, and applications, Crystals 11 (11) (2021) 1317.

[5] F. Staab, Y. Yang, E. Foya, E. Bruder, B. Zingsem, E. Adabifiroozjaei, D. Nasiou, K. Skokov, D. Koch, M. Farle, R.E. Dunin-Borkowski, L. Molina-Luna, O. Gutfleisch, B.-X. Xu, K. Durst, Influence of amorphous phase on coercivity in SmCo5-Cu nanocomposites, Scr. Mater. 240 (2024) 115808.

[6] K. Edalati, Z. Horita, A review on high-pressure torsion (HPT) from 1935 to 1988, Mater. Sci. Eng. A 652 (2016) 325–352.

[7] R. Pippan, S. Scheriau, A. Hohenwarter, M. Hafok, Advantages and limitations of HPT: a review, MSF 584–586 (2008) 16–21.

[8] R. Pippan, S. Scheriau, A. Taylor, M. Hafok, A. Hohenwarter, A. Bachmaier, Saturation of fragmentation during severe plastic deformation, Annu. Rev. Mater. Res. 40 (1) (2010) 319–343.

[9] K. Edalati, D. Akama, A. Nishio, S. Lee, Y. Yonenaga, J.M. Cubero-Sesin, Z. Horita, Influence of dislocation–solute atom interactions and stacking fault energy on grain size of single-phase alloys after severe plastic deformation using high-pressure torsion, Acta Mater. 69 (2014) 68–77.

[10] R.Z. Valiev, Y. Estrin, Z. Horita, T.G. Langdon, M.J. Zehetbauer, Y.T. Zhu, Producing bulk ultrafine-grained materials by severe plastic deformation, JOM 58 (4) (2006) 33–39.

[11] Y.J. Li, X.H. Zeng, W. Blum, Transition from strengthening to softening by grain boundaries in ultrafine-grained Cu, Acta Mater. 52 (17) (2004) 5009–5018.

[12] J. May, H.W. Höppel, M. Göken, Strain rate sensitivity of ultrafine-grained aluminium processed by severe plastic deformation, Scr. Mater. 53 (2) (2005) 189–194.

[13] E. Bruder, P. Braun, Hu. Rehman, R.K. Marceau, A.S. Taylor, R. Pippan, K. Durst, Influence of solute effects on the saturation grain size and rate sensitivity in Cu-X alloys, Scr. Mater. 144 (2018) 5–8.

[14] C. Suryanarayana, D. Mukhopadhyay, S.N. Patankar, F.H. Froes, Grain-size-effects-in-nanocrystalline-materials, J. Mater. Res. 7 (8) (1992) 2114–2118.

[15] H. Gleiter. NANOCRYSTALLINE MATERIALS. Progress in material science 1989; 33:223–315.

[16] C.E. Carlton, P.J. Ferreira, What is behind the inverse Hall–Petch effect in nanocrystalline materials? Acta Mater. 55 (11) (2007) 3749–3756.

[17] R. A. MASUMURA, P. M. HAZZLEDINE and C. S. PANDE. YIELD STRESS OF FINE GRAINED MATERIALS. Acta Metallurgica 1998;46(13):4527–34.

[18] H. Mughrabi, Plastic Deformation and Fracture of Materials, Wiley-VCH, Weinheim (Germany), 1996.

[19] W. Blum, X.H. Zeng, A simple dislocation model of deformation resistance of ultrafine-grained materials explaining Hall–Petch strengthening and enhanced strain rate sensitivity, Acta Mater. 57 (6) (2009) 1966–1974.

[20] W. Blum, X.H. Zeng, Corrigendum to “a simple dislocation model of deformation resistance of ultrafine-grained materials explaining Hall-Petch strengthening and enhanced strain rate sensitivity”, Acta Mater. 59 (15) (2011) 6205–6206.

[21] R.B. Figueiredo, T.G. Langdon, Deformation mechanisms in ultrafine-grained metals with an emphasis on the Hall–Petch relationship and strain rate sensitivity, J. Mater. Res. Technol. 14 (2021) 137–159.

[22] T.G. Langdon. A UNIFIED APPROACH TO GRAIN BOUNDARY SLIDING IN CREEP AND SUPERPLASTICITY. acta metall. mater 1993;42(7):2437–43.

[23] R.B. Figueiredo, Strain-rate sensitivity maps and the estimation of ductility for low temperature superplasticity, J. Mater. Sci. 59 (14) (2024) 5854–5871.

[24] J.H. Schneibel, M. Heilmaier, Hall–petch breakdown at elevated temperatures, Mater. Trans. 55 (1) (2014) 44–51.

[25] R.B. Figueiredo, M. Kawasaki, T.G. Langdon, Seventy years of Hall-Petch, ninety years of superplasticity and a generalized approach to the effect of grain size on flow stress, Prog. Mater Sci. 137 (2023) 101131.

[26] R.B. Figueiredo, T.G. Langdon, Effect of grain size on strength and strain rate sensitivity in metals, J. Mater. Sci. 57 (8) (2022) 5210–5229.

[27] Y. Wang, A. Hamza, E. Ma, Temperature-dependent strain rate sensitivity and activation volume of nanocrystalline Ni, Acta Mater. 54 (10) (2006) 2715–2726.

[28] R. Z. VALIEV, E. V. KOZLOV, YU. F. IVANOV, J. LIAN, A. A. NAZAROV and B. BAUDELET. Deformation behavior of Ultra-Fine-Grained Copper. acta metall. mater 1994;42:2467–75.

[29] K. Zhang, J.R. Weertman, J.A. Eastman, Rapid stress-driven grain coarsening in nanocrystalline Cu at ambient and cryogenic temperatures, Appl. Phys. Lett. 87 (6) (2005).
[30] D.S. Gianola, D.H. Warner, J.F. Molinari, K.J. Hemker, Increased strain rate sensitivity due to stress-coupled grain growth in nanocrystalline Al, Scr. Mater. 55 (7) (2006) 649–652.
[31] W.C. Oliver, G.M. Pharr, An improved technique for determining hardness and elastic modulus using load and displacement sensing indentation, J. Mater. Res. 7 (6) (1992) 1564–1583.
[32] V. Maier, K. Durst, J. Mueller, B. Backes, H.W. Höppel, M. Göken, Nanoindentation strain-rate jump tests for determining the local strain-rate sensitivity in nanocrystalline Ni and ultrafine-grained Al, J. Mater. Res. 26 (11) (2011) 1421–1430.
[33] O. Prach, C. Minnert, K.E. Johanns, K. Durst, A new nanoindentation creep technique using constant contact pressure, J. Mater. Res. 34 (14) (2019) 2492–2500.
[34] C. Minnert, W.C. Oliver, K. Durst, New ultra-high temperature nanoindentation system for operating at up to 1100 °C, Mater. Des. 192 (2020) 108727.
[35] G. Tiphéne, P. Baral, S. Comby-Dassonneville, G. Guillonneau, G. Kermouche, J.-M. Bergheau, W. Oliver, J.-L. Loubet, High-Temperature Scanning Indentation: a new method to investigate in situ metallurgical evolution along temperature ramps, J. Mater. Res. 36 (12) (2021) 2383–2396.
[36] M. Sos, G. Tiphene, J.-L. Loubet, S. Bruns, E. Bruder, K. Durst, Mechanical softening of CuX alloys at elevated temperatures studied via high temperature scanning indentation, Mater. Des. 240 (2024) 112865.
[37] Keil T, Minnert C, Bruder E, Durst K. Solid solution hardening effects on structure evolution and mechanical properties of nanostructured binary and high entropy alloys after high pressure torsion. IOP Conf. Ser.: Mater. Sci. Eng. 2022;1249(1): 12003.
[38] Humphreys FJ, Hatherly M. Recrystallization and related annealing phenomena. 2nd ed. Amsterdam, Boston: Elsevier; 2004.
[39] Humphreys FJ. Recrystallization and Related Annealing Phenomena. Amsterdam Netherlands: Elsevier; 2017.
[40] X. Huang, N. Hansen, N. Tsuji, Hardening by annealing and softening by deformation in nanostructured metals, Science 312 (5771) (2006) 249–251.
[41] T. Keil, S. Taheriniya, E. Bruder, G. Wilde, K. Durst, Effects of solutes on thermal stability, microstructure and mechanical properties in CrMnFeCoNi based alloys after high pressure torsion, Acta Mater. 227 (2022) 117689.
[42] Y.A. Sun, Z.P. Luo, X.Y. Li, K. Lu, Effects of stacking fault energy on deformation induced grain boundary relaxation in nanograined Cu alloys, Acta Mater. 239 (2022) 118256.
[43] X. Zhou, X. Li, K. Lu, 70 nm: the most unstable grain size in Cu prepared by surface mechanical grinding treatment, Nano Mater. Sci. 2 (1) (2020) 32–38.
[44] H. Mecking, U.F. Kocks, Kinetics of flow and strain-hardening, Acta Metall. 29 (11) (1981) 1865–1875.
[45] HSUN HU AND B. B. RATH. On the time exponent in isothermal grain growth. METALLURGICAL TRANSACTIONS 1970;1(3182).
[46] X. Sauvage, G. Wilde, S.V. Divinski, Z. Horita, R.Z. Valiev, Grain boundaries in ultrafine grained materials processed by severe plastic deformation and related phenomena, Mater. Sci. Eng. A 540 (2012) 1–12.
[47] G. Wilde, J. Ribbe, G. Reglitz, M. Wegner, H. Rösner, Y. Estrin, M. Zehetbauer, D. Setman, S. Divinski, Plasticity and grain boundary diffusion at small Grain Sizes, Adv. Eng. Mater. 12 (8) (2010) 758–764.
[48] G. Wilde, S. Divinski, Grain boundaries and diffusion phenomena in severely deformed materials, Mater. Trans. 60 (7) (2019) 1302–1315.
[49] G. T. Horne and R. F. Mehl. Mobilities and diffusion alpha brass. jurnal of metals 1955;(7):88–99.
[50] J.S. Armijo, Self-diffusion in alpha brass, Univ. Arizona (1962).
[51] J. Hino, C. Tomizuka, C. Wert, internal friction and diffusion in 31% alpha brass, Acta Metall. 5 (1957) 41–49.
[52] N.J. Petch, The cleavage strength of polycrystals, J. Iron Steel Inst. 174 (1953) 25–28.
[53] K.K. Ray, K. Chakraborty, On the flow stress/grain size correlation in copper and alpha-brass, J. Mater. Sci. Lett. 15 (1996) 727–730.
[54] J. Bach, J.P. Liebig, H.W. Höppel, W. Blum, Influence of grain boundaries on the deformation resistance: insights from an investigation of deformation kinetics and microstructure of copper after predeformation by ECAP, Phil. Mag. 93 (35) (2013) 4331–4354.
[55] N. Ahmed, A. Hartmaier, Mechanisms of grain boundary softening and strain-rate sensitivity in deformation of ultrafine-grained metals at high temperatures, Acta Mater. 59 (11) (2011) 4323–4334.
[56] K. Durst, V. Maier, Dynamic nanoindentation testing for studying thermally activated processes from single to nanocrystalline metals, Curr. Opin. Solid State Mater. Sci. 19 (6) (2015) 340–353.
[57] Q. Wei, S. Cheng, K. Ramesh, E. Ma, Effect of nanocrystalline and ultrafine grain sizes on the strain rate sensitivity and activation volume: fcc versus bcc metals, Mater. Sci. Eng. A 381 (1–2) (2004) 71–79.
[58] S. Laube, A. Kauffmann, F. Ruebeling, J. Freudenberger, M. Heilmaier, C. Greiner, Solid solution strengthening and deformation behavior of single-phase Cu-base alloys under tribological load, Acta Mater. 185 (2020) 300–308.
[59] V. Maier-Kiener, X. An, L. Li, Z. Zhang, R. Pippan, K. Durst, Influence of solid solution strengthening on the local mechanical properties of single crystal and ultrafine-grained binary Cu–Al X solid solutions, J. Mater. Res. 32 (24) (2017) 4583–4591.
[60] R.J. Asaro, S. Suresh, Mechanistic models for the activation volume and rate sensitivity in metals with nanocrystalline grains and nano-scale twins, Acta Mater. 53 (12) (2005) 3369–3382.